

Influence of electrical impedance and mechanical bistability on Galfenol-based unimorph harvesters

Zhangxian Deng and Marcelo J Dapino

Abstract

A study on iron-gallium (Galfenol) unimorph harvesters is presented which is focused on extending the power density and frequency bandwidth of these devices. A thickness ratio of 2 (ratio of substrate to Galfenol thickness) has been shown to achieve maximum power density under base excitation, but the effect of electrical load capacitance on performance has not been investigated. This article experimentally analyzes the influence of capacitive electrical loads and extends the excitation type to tip impulse. For resistive-capacitive electrical loads, the maximum energy conversion efficiency achieved under impulsive excitation is 5.93%, while the maximum output power and output power density observed for a 139.5 Hz, 3 m/s² amplitude sinusoidal base excitation is 0.45 W and 6.88 mW/cm³, respectively, which are 8% higher than those measured under purely resistive loads. A finite element model for Galfenol unimorph harvesters, which incorporates magnetic, mechanical, and electrical dynamics, is developed and validated using impulsive responses. A buckled unimorph beam is experimentally investigated. The proposed bistable system is shown to extend the harvester's frequency bandwidth.

Keywords

Galfenol, unimorph, COMSOL multiphysics, energy harvesting, bistable

Introduction

Magnetostrictive iron-gallium alloys (Galfenol) are a class of smart materials that exhibit moderate magnetostriction (around 400 ppm) and magnetization (1200 kA/m). Galfenol has a relatively high tensile strength compared to other adaptive materials such as Terfenol-D and piezoelectric ceramics. Hence, it is robust even when subjected to combined loading.

With the development of integrated circuits, recent embedded or wireless sensors have experienced a reduction in size and energy consumption. Built-in power sources for those devices eliminate the need for frequent battery replacement. Vibration-based energy harvesters are able to scavenge structural vibration and convert it to useful electrical energy. Galfenol exhibits strong magneto-mechanical coupling, and thus it is attractive for implementation in energy harvester designs. Staley and Flatau (2005) investigated the energy harvesting properties of Galfenol under various bias conditions. Ueno and Yamada (2011) experimentally analyzed a bimorph harvester that consists of two Galfenol layers bonded together and evaluated its energy conversion efficiency by applying impulsive tip excitations. Berbyuk (2013) developed a Galfenol-based


energy harvester in axial mode and achieved 338 mW/cm³ power density. Deng and Dapino (2015a) conducted experiments on Galfenol unimorph energy harvesters considering various design parameters such as load resistance, beam thickness ratio, and bias magnetic field strength.

Unlike piezoelectric energy harvesters, Galfenol harvesters are low output impedance voltage sources and as such, they can directly drive electrical loads without management circuits. Past studies (Berbyuk, 2013; Deng and Dapino, 2015a; Ueno and Yamada, 2011) have focused on purely resistive loads. However, the output power capacity of a harvester can be improved by connecting capacitors in parallel with the load resistor and creating a resonant resistive-inductive-capacitive (RLC) circuit. A comprehensive system level model for Galfenol unimorphs that couples magnetic,

Department of Mechanical and Aerospace Engineering, The Ohio State University, USA

Corresponding author:

Marcelo Dapino, Department of Mechanical and Aerospace Engineering, The Ohio State University, Columbus, OH 43210, USA.
Email: dapino.1@osu.edu

Journal of Intelligent Material Systems and Structures
2017, Vol. 28(3) 421–431
© The Author(s) 2016
Reprints and permissions:
sagepub.co.uk/journalsPermissions.nav
DOI: 10.1177/1045389X16666176
journals.sagepub.com/home/jim


mechanical, and electric dynamics, is essential for computationally determining the load impedance that maximizes electrical power production for a given vibration input. Yoo and Flatau (2012) presented a lumped parameter model for unimorph energy harvesters based on linearized magnetomechanical equations. Zhao and Lord (2006) included eddy currents and electrical dynamics as part of linearized piezomagnetic equations and theoretically quantified the maximum output power of Galfenol-based energy harvesters at high frequencies. However, linear equations are not accurate enough to describe Galfenol in nonlinear regimes that include material anisotropy, hysteresis, and saturation.

More sophisticated models based on thermodynamic principles have been developed. Shu et al. (2011) combined a discrete energy averaged model (Armstrong, 2003; Evans and Dapino, 2010) with 2D Euler beam theory and created a finite element model for Galfenol unimorphs driven under constant magnetic fields. Chakrabarti and Dapino (2011) developed a 3D fully nonlinear anhysteretic finite element model for a Galfenol unimorph actuator. Deng and Dapino (2014) later added material hysteresis to this model. To improve model efficiency, Rezaeealam et al. (2012) presented a 2D finite element model in which Galfenol nonlinearities were described through calculated nonlinear lookup tables. Deng and Dapino (2015a) utilized the discrete energy averaged model to generate the lookup tables and proposed a systematic optimization procedure for Galfenol unimorph harvesters. However, none of the current finite element approaches include the electrical dynamics.

One of the key challenges for a structural vibration energy harvester is to perform energy effectively over a broad frequency bandwidth, since the power spectrum of practical vibration sources are usually wideband and dependent on operating conditions (Roundy et al., 2003). Moon and Holmes (1979) numerically analyzed a bistable cantilever beam, which has two equilibrium positions due to the nonlinear magnetic force applied on its tip. Depending on the excitation energy, the cantilever beam is able to operate in a low-energy orbit (around one of the equilibrium positions), in a chaotic regime, and in a high-energy orbit (around two equilibrium positions). Broadband energy harvesters have been developed based on the chaotic and high-energy orbit responses. Harne and Wang (2013) reviewed several bistable systems that have been implemented in piezoelectric cantilever harvesters. Erturk et al. (2009) and Ferrari et al. (2010) have used chaotic responses to increase the frequency bandwidth of a magnetoelastic beam harvester and a piezoelectric cantilever harvester, respectively. Erturk and Inman (2011) later implemented the high-energy orbit to expand the frequency bandwidth of the piezoelectric cantilever harvester. However, their work was confined to soft beams due to

the limited magnetic force available. Van Blarigan et al. (2012) connected a buckled beam to the tip of the cantilever and observed a significant frequency bandwidth increment for stiffer beams.

In this study, a Galfenol unimorph beam with a natural frequency of 139.5 Hz and a thickness ratio of 2 is first tested by applying impulsive tip deflections, and the energy conversion efficiency η is evaluated experimentally under purely resistive and resistive-capacitive electrical loadings. A fully nonlinear, 2D finite element (FE) model, incorporating mechanical, magnetic, and electrical dynamics, is developed based on calculated nonlinear lookup tables to describe the impedance matching results. The same unimorph is then subjected to a 139.5 Hz, 3 m/s² amplitude sinusoidal base excitation under purely resistive and resistive-capacitive loads, and its average output power and average output power density are measured. To extend the system frequency bandwidth, a bistable buckled Galfenol unimorph beam is tested under sinusoidal base excitations. Since a softer beam requires less buckling force and the depth of each of its two energy wells is less sensitive to the buckling magnitude, the buckled Galfenol unimorph beam investigated has a thickness ratio of 2/3.

Theory

Figure of merit

Different figures of merit have been defined for energy harvesters. In this study, four definitions are employed. Energy conversion efficiency η is defined as

$$\eta = \frac{E_{\text{out}}}{E_{\text{in}}} \quad (1)$$

where E_{out} is the energy consumed or stored by the electrical circuit and E_{in} is the mechanical energy input. Ueno and Yamada (2011) utilized this definition for impulsive tip excitation and $E_{\text{in}} = 0.5F_0D_0$, where F_0 is the static force and D_0 is the initial tip deflection due to the applied force. Kita et al. (2015) later adapted the same definition for periodic base excitation. However, the mechanical energy E_{in} available from structural vibration sources is essentially unlimited (because time is unlimited), hence the definition given by equation (1) is meaningless for periodic excitations. The value of η in this work is presented only for comparison with previous impulsive studies (Kita et al., 2015; Ueno and Yamada, 2011).

Average power output \bar{P} is defined as

$$\bar{P} = \frac{1}{T} \int_0^T \frac{V^2(t)}{R_L} dt \quad (2)$$

where R_L is the load resistance, $V(t)$ is the voltage across R_L , and T is the period of $V(t)$.

Average output power density PD is defined as

$$PD = \frac{\bar{P}}{V_a} \quad (3)$$

where V_a is the volume of the active material. Power density has been widely used in previous literature.

Normalized power density PD is defined as

$$|PD| = PD/f^2 \quad (4)$$

where f denotes the frequency of a sinusoidal base excitation. For a given amplitude, the power of the sinusoidal vibration source is proportional to f^2 , hence the normalized power density $|PD|$ effectively eliminates the difference of the vibration sources.

Electrical dynamics and impedance matching

Figure 1 shows the equivalent circuit for a typical Galfenol harvester. The resistance and inductance of the pickup coil are denoted by R_c and L_c , respectively. An electrical load consisting of R_L and C_L is connected to the coil. The resistor R_L represents the load resistance of energy storage components, hence the energy consumed by R_L is usually considered as the energy harvested by the device. The capacitor C_L completes the RLC circuit that helps to increase the power dissipated on R_L . The voltage $V(t)$ represents the induced voltage across the pickup coil at open circuit. The induced current I flows through the coil and generates magnetic field along the length of the beam.

Assuming that the input voltage $V(t)$ is sinusoidal and its angular frequency is ω_e , the average power dissipated on the resistor is

$$\begin{aligned} \bar{P} &= \frac{1}{T} \int_0^T \frac{V^2(t)}{R_L} dt \\ &= \frac{V_{\text{amp}}^2}{2} \frac{1}{2R_c + (L_c^2 C_L^2 \omega_e^4 + R_c^2 C_L^2 \omega_e^2 - 2L_c C_L \omega_e^2 + 1)R_L + (L_c^2 \omega_e^2 + R_c^2)/R_L} \end{aligned} \quad (5)$$

where V_{amp} and T are the amplitude and period of $V(t)$, respectively. Previous studies focused on purely resistive electrical loading ($C_L = +\infty$) (Deng and Dapino, 2015a). The maximum average output power is

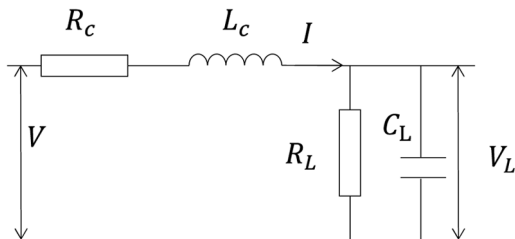


Figure 1. Equivalent circuit for the pickup coil and the electrical load.

$$\max(\bar{P}|_{C_L = +\infty}) = \frac{V_{\text{amp}}^2}{4} \frac{1}{R_c + \sqrt{R_c^2 + L_c^2 \omega_e^2}} \quad (6)$$

where $R_L = \sqrt{R_c^2 + L_c^2 \omega_e^2}$. For resistive-capacitive electrical loading, the maximum power output

$$\max(\bar{P}) = \frac{V_{\text{amp}}^2}{8R_c} \quad (7)$$

which occurs for

$$C_L = \frac{L_c}{L_c^2 \omega_e^2 + R_c^2} \quad \text{and} \quad R_L = \frac{R_c^2 + L_c^2 \omega_e^2}{R_c} \quad (8)$$

Since $L_c > 0$,

$$\max(\bar{P}|_{C_L = 0}) < \frac{V_{\text{amp}}^2}{4} \frac{1}{2R_c} = \max(\bar{P}) \quad (9)$$

Equation (9) shows that the capacitor C_L is able to improve the output power of the energy harvester. Deng and Dapino (2015b) experimentally demonstrated the benefits of the capacitor C_L connected in parallel for impulsive tip excitations. This study considers sinusoidal base excitation and investigates the power output under various resistive-capacitive loadings.

FE model with fully-coupled mechanical, magnetic, and electrical dynamics

Figure 2 depicts the coupling among mechanical, magnetic, and electrical domains for Galfenol unimorph harvesters, where the same notation found in previous studies (Deng and Dapino, 2014, 2015a) is used. In the mechanical domain, V_u is the volume of Galfenol and other passive materials in the load path, \mathbf{T} is the stress tensor, \mathbf{S} is the strain tensor, ρ is the material density, c is the material damping coefficient, \mathbf{u} is the displacement vector, \mathbf{t} is the surface traction, and \mathbf{f}_B is the body force. In the magnetic domain, V_B is the volume of the magnetostrictive system and the surrounding air, \mathbf{H} is the magnetic field vector, \mathbf{B} is magnetic flux density vector, \mathbf{A} is the magnetic vector potential, σ is the electrical conductivity, \mathbf{J}_s is the current density inside the coil wire, and \mathbf{n} is the unit direction vector of surface ∂V_B . In the electrical domain, the circuit impedance $Z(\mathbf{H}, \mathbf{T})$ is written as a function of stress and magnetic field. The nonlinear constitutive functions of Galfenol are $H_{xx}(|B_x|, T_{xx})$ and $\lambda_{xx}(H_x, T_{xx})$, where H_x , B_x , T_{xx} , and λ_{xx} are the magnetic field, flux density, stress, and magnetostriction along the x-axis, respectively. The symbols N_c , A_c , and \mathbf{n}_c represent the coil's turns, cross-section, and normal direction of coil axis, respectively. The current through the pickup coil induces an opposing magnetic field \mathbf{H}_b . Deng and Dapino (2014) developed a finite element model where the mechanical and magnetic domains are two-way coupled. Deng and Dapino

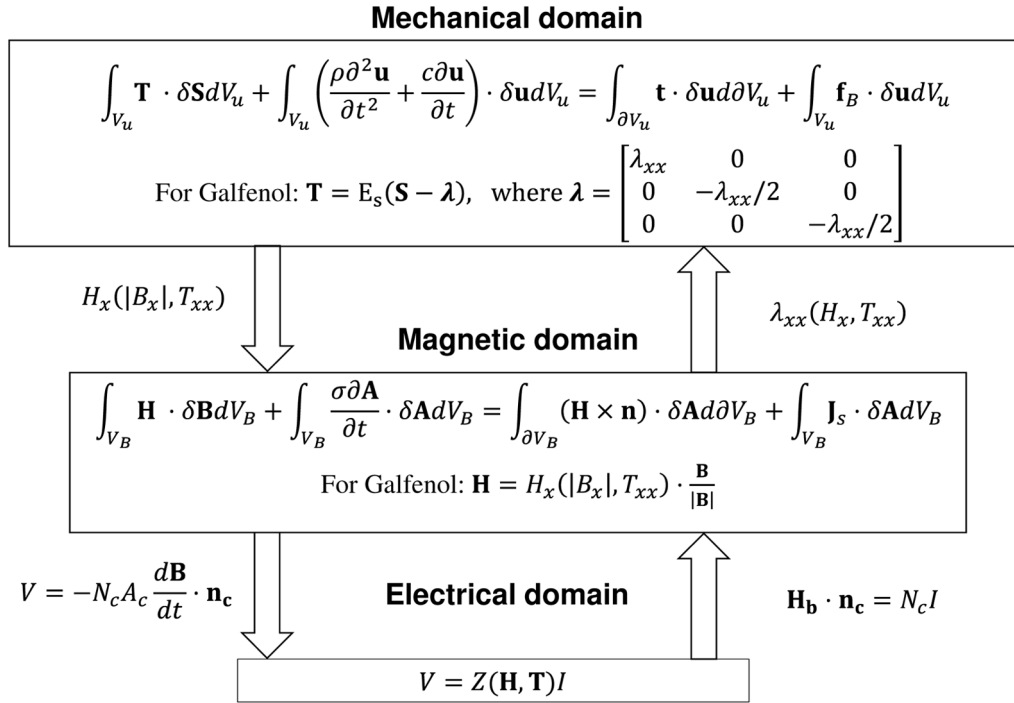


Figure 2. Flowchart of fully coupled mechanical, magnetic, and electrical dynamics.

(2015a) incorporated electrical dynamics into the FE structure. However, three assumptions were made which effectively limited the interactions between the magnetic and electrical domains to a one-way coupling. These assumptions are:

1. the magnetic field caused by the induced current through the pickup coil was ignored;
2. only the fundamental component of the voltage $V(t)$ was considered;
3. the permeability of the Galfenol element was assumed to be constant in the electrical domain, thus the circuit impedance $Z(\mathbf{H}, \mathbf{T})$ was constant.

The model uncertainty associated with each assumption is defined as the percentage difference between the model output with a given assumption in place and the model output without the same assumption. The uncertainty calculated for each of the above assumptions are 7.7%, 2.8%, and 5.8%, respectively. This information allows us to estimate the effect of each assumption and to potential lift (or not) a given assumption in the interest of accuracy in lieu of computational speed. Further details on the implications of these assumptions are provided in the article by Deng and Dapino (2015b). In this article, the three assumptions are lifted leading to complete elimination of these sources of modeling uncertainty. The electrical circuit is described as

$$\begin{aligned} V &= IR_c + L_c(\mathbf{H}, \mathbf{T}) \frac{dI}{dt} + V_L \\ I &= \frac{1}{R_L} V_L + C \frac{dV_L}{dt} \end{aligned} \quad (10)$$

where V and I can be associated with magnetic domain using Maxwell's equations (Chakrabarti and Dapino, 2011; Deng and Dapino, 2014). By incorporating equation (10) within our previous FE model, Ampere's law is taken into account and the voltage V includes fundamental, as well as higher order components. The circuit impedance $Z(\mathbf{H}, \mathbf{T})$, which is related to the stress- and field-dependent Galfenol permeability, is written as a function of magnetic field \mathbf{H} and stress tensor \mathbf{T} . This approach is in contrast to that used previously, in which the assumption of a constant inductance implied constant Galfenol permeability.

Thin elastic layer

A previous FE model for Galfenol unimorphs assumes that the Galfenol layer is rigidly connected to the stainless steel substrate (Deng and Dapino, 2015a). In practice, both layers are bonded together using strain gauge glue (M-bond 200) with a modulus of about 9 MPa. This thin glue layer (≈ 0.0254 mm) reduces the overall stiffness of the beam thus it affects the system's dynamic response. Directly modeling the glue layer as a 3D subdomain requires an extremely fine mesh which greatly increases the computational burden. Deng and Dapino

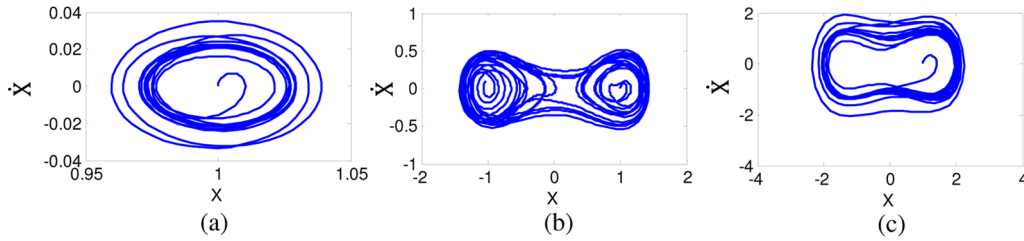


Figure 3. Phase plot of the standard Duffing equation (15), where $\Omega = 0.8$, $\gamma = 0.1$, and initial condition $(\dot{X}_0, X_0) = (0, 1)$ (a) $f = 0.01$ (b) $f = 0.1$ (c) $f = 0.15$.

(2015b) decoupled the geometric continuity between the Galfenol and substrate layers, and connected them by an elastic force \mathbf{F}_e and a viscous force \mathbf{F}_v

$$\begin{aligned}\mathbf{F}_e &= \mathbf{k}\Delta\mathbf{u} \\ \mathbf{F}_v &= \mathbf{c}\Delta\dot{\mathbf{u}}\end{aligned}\quad (11)$$

where $\Delta\mathbf{u}$ is the relative displacement between the two layers. The terms \mathbf{k} and \mathbf{c} are the stiffness and the damping matrices of the glue layer, respectively. The force on the glue layer σ_g satisfies

$$\sigma_g \mathbf{n}_g = -\mathbf{F}_e - \mathbf{F}_v \quad (12)$$

where \mathbf{n}_g is the unit norm vector of the glue layer.

Duffing's equation

The cantilever unimorph beam exhibits dramatic deflection only if the excitation frequency is close to the beam's natural frequency. Bistable systems, for example buckled beams, transform from one stable state to the other thus creating large amplitude motion. This nonlinear action can be described by

$$m\ddot{x} + c\dot{x} + kx = mA_0 \cos(\omega t) + F_y(x) \quad (13)$$

where m , c , and k are the equivalent inertia, damping, and stiffness, respectively. The base excitation amplitude is A_0 and the excitation frequency is ω . The nonlinear magnetic force on the tip $F_y(x)$ is estimated as an odd polynomial function of tip displacement x

$$F_y(x) = a_1x + a_3x^3 + h(x^5) \quad (14)$$

Equation (13) can be written as the standard Duffing equation by rescaling the time t and displacement x

$$\ddot{X} + \gamma\dot{X} - \frac{1}{2}(1 - X^2)X = f \cos(\Omega\tau) \quad (15)$$

where

$$\begin{aligned}X &= x/a_0, \tau = t/\omega_0, \gamma = C\omega_0/M \\ f &= A_0\omega_0^2/a_0, \Omega = \omega/\omega_0 \\ a_0 &= \left(\frac{K - a_1}{a_3}\right)^{1/2}, \omega_0 = \left(\frac{0.5M}{a_1 - K}\right)^{1/2}\end{aligned}\quad (16)$$

Depending on the excitation frequency and amplitude, the behavior of the Duffing equation can either be periodic or chaotic. When the excitation is small, the cantilever beam oscillates in a low-energy orbit, which is around one of the equilibrium positions, as shown in Figure 3(a). As the excitation energy increases, the cantilever beam is able to chaotically jump between two equilibrium positions (Figure 3(b)) and ultimately reach a high-energy orbit surrounding both equilibrium positions (Figure 3(c)). In this study, the high-energy orbit is used to improve the frequency bandwidth of Galfenol-based unimorph harvesters at relatively high frequencies (>100 Hz) due to the large force obtained from buckling.

Results and discussion

Multiphysics modeling and impulsive response

Experimental setup. Figure 4 shows the experimental setup that is used to evaluate the performance of a unimorph harvester under impulsive tip deflection. A $38.1 \text{ mm} \times 6.35 \text{ mm} \times 0.381 \text{ mm}$ polycrystalline Galfenol beam (with 18.4% gallium) manufactured by Etrema Products, Inc. is bonded to a 316 stainless steel beam ($38.1 \text{ mm} \times 6.35 \text{ mm} \times 0.762 \text{ mm}$). The Galfenol beam was rolled from an as-grown bulk rod and heat treated afterward, thus no pre-stress was built into the material.

A design parameter that affects the energy harvesting capacity is the beam thickness ratio, which is defined as the thickness of the substrate layer over the thickness of the Galfenol layer. Previous experiments have shown that a beam with a thickness ratio of 2 generates maximum output power for the selected magnetostrictive material and the unimorph beam configuration (Deng and Dapino, 2015a). Hence, experiments in this study are conducted on a beam with a thickness ratio of 2. About 11.43 mm of the unimorph beam is constrained inside the aluminum fixture, so the effective length of the Galfenol layer is 26.67 mm. A 3.68 g stainless steel inertia mass is glued on the beam's tip, and two permanent magnets with a remnant flux density of about 1.1 T are attached to generate a bias magnetic field. A 1-inch-long, 1100 turns pickup coil made of AWG 36 copper wire with a resistance of 56.2Ω is wound around the unimorph beam. The tip deflection is measured by a

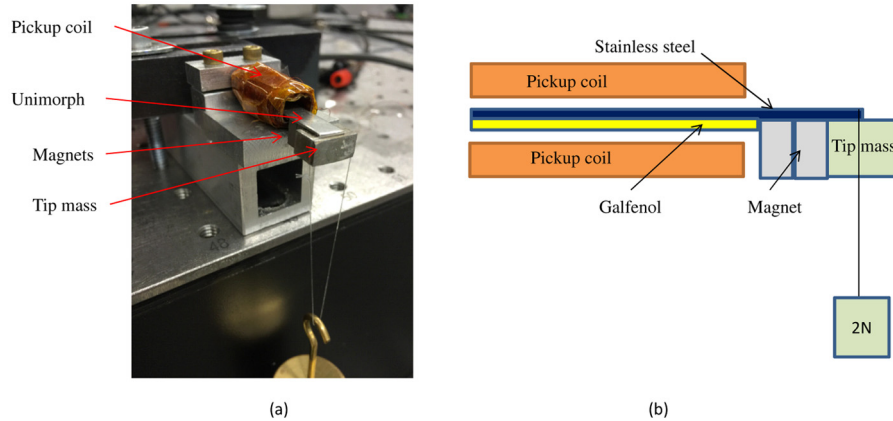


Figure 4. (a) Experiment setup; (b) cross-sectional view of the unimorph harvester.

Keyence LK-G32 laser position sensor. A resistance decade box ($\pm 1\%$ accuracy) and a capacitance decade box ($\pm 5\%$ accuracy) are used to adjust the load impedance. Voltage across the resistor and the tip deflection signals are sent to a SignalCalc dynamic signal analyzer at a 5.12 kHz sampling rate.

Open circuit. A 2 N mass is hung on the tip of the unimorph beam, as shown in Figure 4. The unimorph undergoes an impulsive response as soon as the fishing wire is cut. The tip deflection $D(t)$ decays exponentially as

$$D(t) = D_{\text{tip}} e^{-2\pi\xi f_r t} \cos(2\pi\sqrt{1 - \xi^2} f_r t) \quad (17)$$

where ξ is the damping ratio and f_r is the beam's natural frequency. Figure 5 shows that equation (17) can accurately describe the decay of the tip displacement with $f_r = 139.5$ Hz and $\xi = 0.0045$. Since no resistors are connected to the pickup coil, the mechanical energy is dissipated through structural damping and Galfenol hysteresis loss. These energy losses were simulated through Rayleigh damping (Deng and Dapino, 2015a; Shu et al., 2011) in the finite element model.

Previous studies (Chakrabarti and Dapino, 2011; Shu et al., 2011, 2014) solved the dynamic FE model in the time domain directly using the backward differentiation formula (BDF) method. This method introduces numerical damping to filter out high frequency components, thus improving model convergence. However, an ideal impulsive input signal, which has broadband frequency content, excites all modes of the beam. Hence, the model will have significant error if the high frequency modes are eliminated by the BDF method. This study implements the BDF – α method that is able to control the numerical damping (Chung and Hubert, 1993).

Figures 6 and 7 present the impulsive responses of the tip deflection $D(t)$ and voltage V_L under open circuit

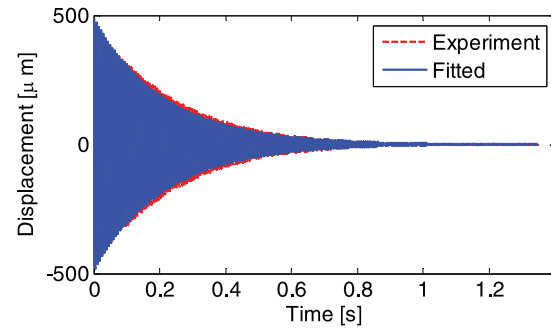


Figure 5. Comparison of the experimental impulsive response (open circuit) and model calculation for the tip deflection.

condition. The proposed finite element model is able to accurately describe the dynamic response for open circuit conditions.

Purely resistive loading

The electrical circuit described in equation (10) is represented by SPICE netlists in COMSOL Multiphysics. Figure 8 shows the energy conversion efficiency η of the Galfenol unimorph when only R_L is connected. The maximum $\eta = 5.52\%$ when $R_L = 74\Omega$. The finite element model is able to closely fit the decay of the tip deflection for a purely resistive electrical load (Figure 9). The output voltage is also accurately calculated except for a slight phase lead observed in Figure 10. This phase difference is possibly due to the modeling error of the pickup coil's inductance.

Resistive-capacitive loading. Equation (8) proves that the output power of the unimorph beam harvester can be improved by connecting a capacitor in parallel with the resistive load. Figure 11 shows the experimental results of η for various C_L values when $R_L = 74\Omega$. The maximum $\eta = 5.93\%$ when a $2\mu\text{F}$ capacitor is attached and the η is improved by 7.4%.

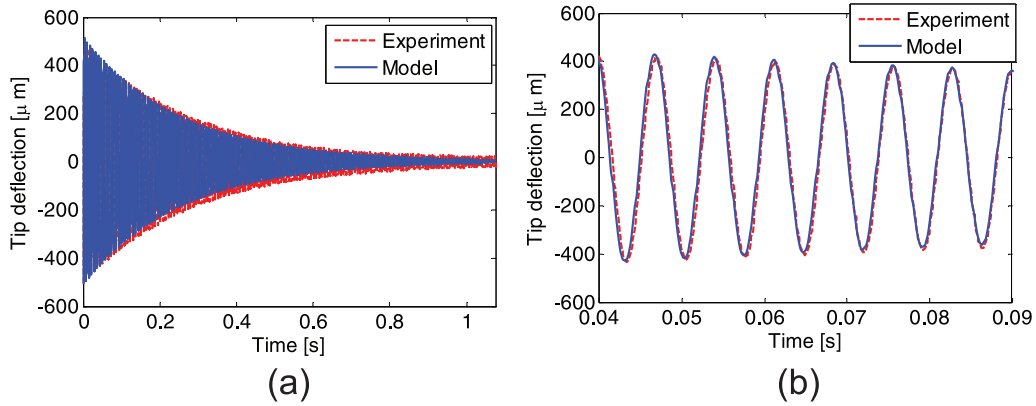


Figure 6. Open circuit response. (a) Impulsive response (tip deflection) of the unimorph; (b) zoomed in view of the tip deflection (0.04–0.09 s).

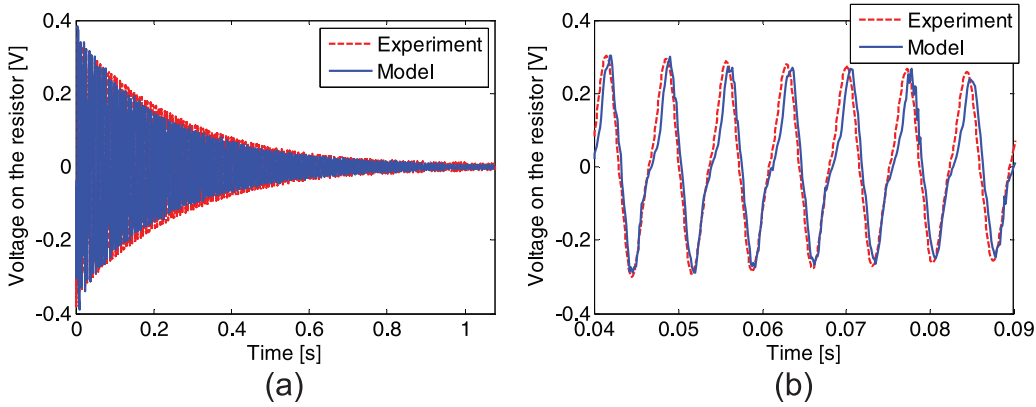


Figure 7. Open circuit response. (a) Impulsive response of open circuit voltage; (b) zoomed in view of the output voltage (0.04–0.09 s).

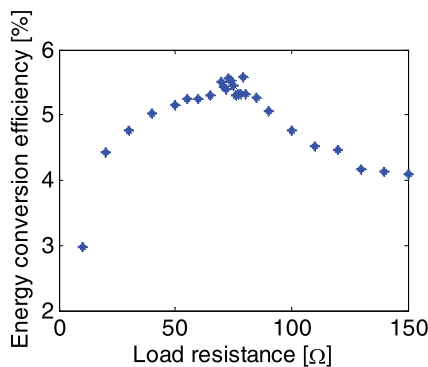


Figure 8. Energy conversion efficiency η with respect to different load resistance.

Figure 12 shows that the finite element model can accurately describe the decay of the tip deflection under resistive-capacitive loading conditions. However, there exists a slight phase lag in Figure 13. The modeling error of the coil inductance, as well as the accuracy of the capacitor decade box ($\pm 5\%$), contributes to this phase difference.

Impedance matching

Experimental setup. The Galfenol unimorph harvester (Figure 4) is placed on the electromagnetic shaker as shown in Figure 14. An aluminum stage separates the harvester from the electromagnetic shaker with the purpose of minimizing the effect of stray fields from the shaker on the harvester. The system was tested in two ways: In one test, the pickup coil was placed above the aluminum stage without the unimorph in place. When the shaker was on, the output voltage from the coil was extremely low, buried in floor noise. Hence, the stray flux has no measurable influence on the pickup coil. The second test consisted of measuring the magnetic field on the Galfenol layer when the unimorph was placed on top of the aluminum stage without bias permanent magnets at the tip of the beam. The measured field was negligible, indicating that stray fields have no measurable influence on the unimorph.

Results. A 139.5 Hz, 3 m/s² amplitude base excitation frequency is applied in order to drive the unimorph

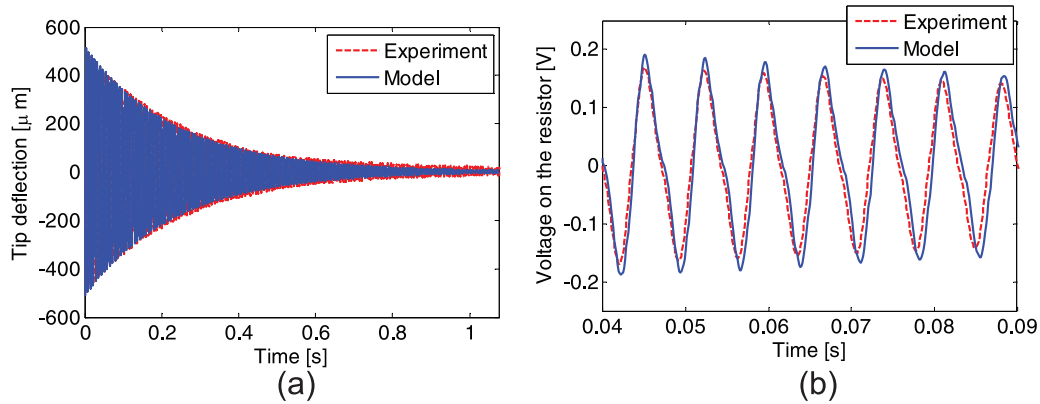


Figure 9. Load resistance $R_L = 74\Omega$. (a) Impulsive response (tip deflection) of the unimorph; (b) zoomed in view of the tip deflection (0.04–0.09 s).

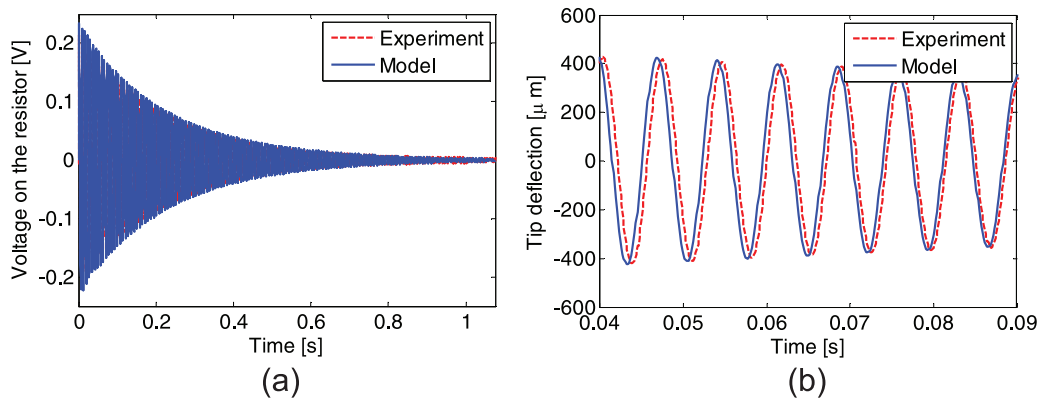


Figure 10. Load resistance $R_L = 74\Omega$. (a) Impulsive response of V_L when $R_L = 74\Omega$; (b) zoomed in view of the output voltage (0.04–0.09 s).

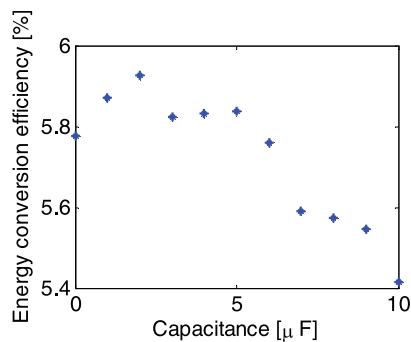


Figure 11. Energy conversion efficiency η with respect to different load capacitance when $R_L = 74\Omega$.

beam near its resonance frequency. According to the results presented in Figure 15, the maximum average power \bar{P}_{\max} and average output power density PD_{\max} are 0.41 W and 6.37 mW/cm³, respectively, for a purely resistive load $R_L = 74\Omega$ ($C_L = +\infty$). The values of \bar{P}_{\max} and PD_{\max} are improved to 0.45 W and 6.88 mW/cm³, respectively, when the load impedance consists of $R_L = 66\Omega$ and $C_L = 2\mu F$. Hence, the power output

capability is improved by 8%, through creating a resonant RLC circuit.

Buckled beam

Experimental setup. Application of a nonlinear force on the tip of a cantilever beam converts the beam to a bistable system and improves the frequency bandwidth. This work investigates a unimorph beam as shown in Figure 16, where the nonlinear tip force is applied through a buckled beam structure. The same aluminum fixtures, as presented in Figure 14, are used to constrain the beam. The length of the stainless steel layer is twice the Galfenol's length. The thickness ratio of the unimorph beam is 2/3 such that less buckling force is required and the depth of each of the beam's two energy wells is less sensitive to the buckling magnitude. The distance between the two fixtures are tuned manually. Experimental results are compared between buckled unimorph and a Galfenol unimorph cantilever with the same thickness ratio under 9.8 m/s² amplitude sinusoidal base excitations.

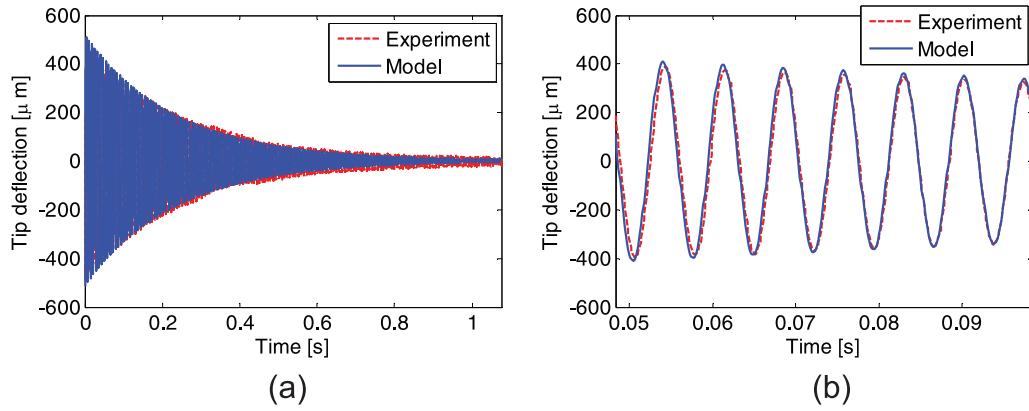


Figure 12. Impulsive response when $R_L = 74\Omega$ and $C_L = 2\mu\text{F}$. (a) Impulsive response (tip deflection) of the unimorph; (b) zoomed in view of the tip deflection (0.04—0.09 s).

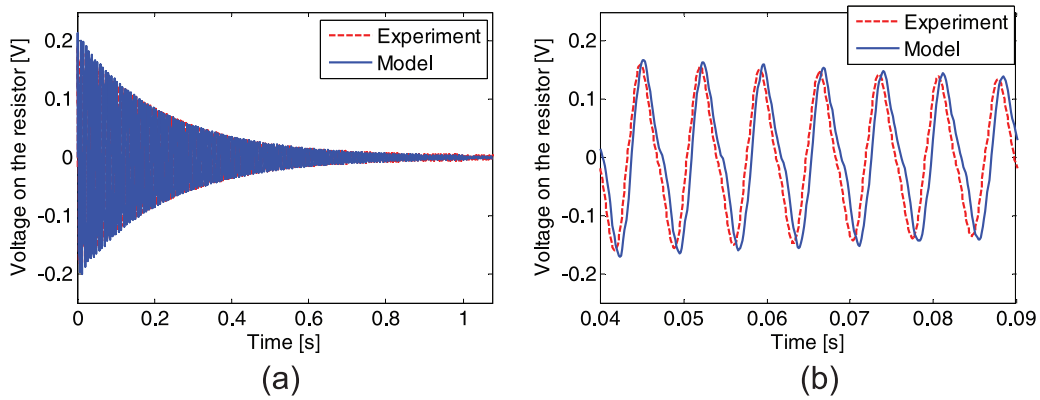


Figure 13. Impulsive response when $R_L = 74\Omega$ and $C_L = 2\mu\text{F}$. (a) Impulsive response (voltage across the resistor) of the unimorph; (b) zoomed in view of the output voltage (0.04—0.09 s).

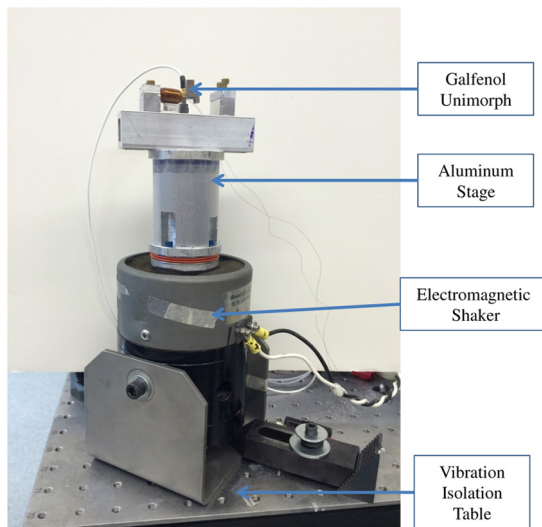


Figure 14. View of the shaker, mounting and isolation stages, and unimorph beam.

Results. Since the buckled and cantilever unimorph beams have different natural frequencies, the normalized power density is used to eliminate the source differences. Figure 17 shows a comparison of the measured $|PD|$ values in the frequency domain for both beams. The cantilever beam approximately behaves as a lightly-damped, second-order system. The buckled beam exhibits a typical hardening effect, which is similar to the nonlinear behavior observed in buckled piezoelectric beam harvesters (Cottone et al., 2012).

As a lightly-damped linear system, the frequency bandwidth of the cantilever beam can be directly estimated from the half-power points as 1.5 Hz. Employing the same definition to estimate the frequency bandwidth of the buckled beam, 10.5 Hz is obtained. Over the passband, a lower net available output power density is obtained in the latter case. To simultaneously incorporate the effect of $|PD|$ and the frequency bandwidth, the gain-bandwidth product

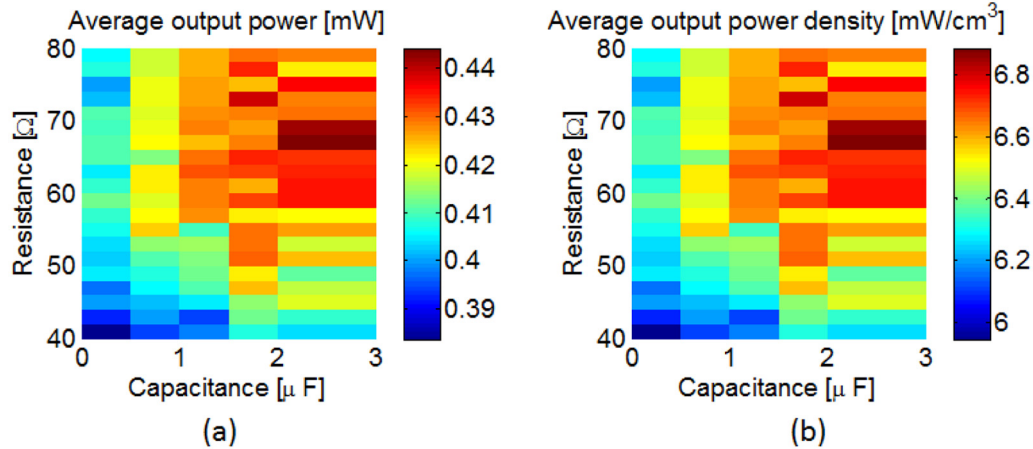


Figure 15. (a) Average output power and (b) average output power density versus load resistance and capacitance for a Galfenol unimorph beam with a thickness of 2 under 3 m/s^2 amplitude, 139.5 Hz base excitation.

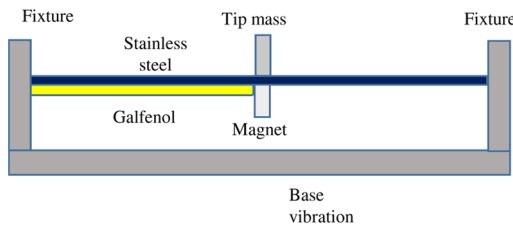


Figure 16. 2D geometry for buckled Galfenol unimorph beam.

(GB) is considered as the product of the harvester's bandwidth and the maximum $|PD|$. The values of GB measured from the cantilever beam and the buckled beam are $1.49 \times 10^{-3} \text{ mW}/(\text{cm}^3 \cdot \text{Hz})$ and $1.76 \times 10^{-3} \text{ mW}/(\text{cm}^3 \cdot \text{Hz})$, respectively. Although the buckled beam has a lower net available $|PD|$, its ability to generate power is higher than the cantilever beam over its frequency passband.

Concluding remarks

This study first experimentally quantified the performance of a Galfenol-based unimorph energy harvester (thickness ratio of 2) under impulsive excitations in terms of energy conversion efficiency. When purely resistive loads were connected to the pickup coil, the maximum η (at $R_L = 74 \Omega$) is 5.52%. Connecting a $2 \mu\text{F}$ capacitor in parallel with the resistive load increased the value of η to 5.93% (by 7.4%). The same unimorph harvester was then tested for 139.5 Hz, 3 m/s^2 base excitations under purely resistive and resistive-capacitive load. The maximum average output power \bar{P}_{\max} and average output power density PD_{\max} are 0.45 W and $6.88 \text{ mW}/\text{cm}^3$, respectively, when a 66Ω resistor and a $2 \mu\text{F}$ capacitor are in parallel. Compared to the results obtained under purely resistive loads, the capacitive-resistive load improved the power output capability by 8%. A 2D finite element model,

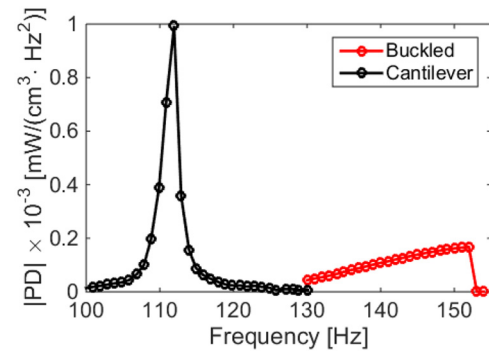


Figure 17. Comparison of the frequency response of a cantilever Galfenol unimorph beam and a buckled Galfenol unimorph beam.

considering mechanical, magnetic, and electrical dynamics of the unimorph system, was proposed and validated using the impulsive responses. Based on the proposed model, a parametric study targeting maximum power output can be developed in the future. A bistable buckled unimorph beam was validated experimentally for frequency bandwidth expansion. The frequency bandwidth of a 2/3 thickness ratio unimorph harvester was improved from 1.5 Hz to 10.5 Hz, by manually adjusting the buckling force. The relationship between frequency bandwidth and buckling magnitude needs to be investigated in future studies.

Declaration of Conflicting Interest

The authors declare that there is no conflict of interest.

Funding

The author(s) disclosed receipt of the following financial support for the research, authorship, and/or publication of this article: Funding was provided by the member organizations of the Smart Vehicle Concepts Center, a National

Science Foundation Industry/University Cooperative Research Center (www.SmartVehicleCenter.org) established under NSF Grant IIP-1238286.

References

- Armstrong WD (2003) An incremental theory of magnetoelastic hysteresis in pseudo-cubic ferro-magnetostrictive alloys. *Journal of Magnetism and Magnetic Materials* 263(1): 208–218.
- Berbyuk V (2013) Vibration energy harvesting using Galfenol-based transducer. Proceedings of SPIE 8688: 86881F.
- Chakrabarti S and Dapino MJ (2011) Nonlinear finite element model for 3D Galfenol systems. *Smart Materials and Structures* 20(10): 105034.
- Chung J and Hubert GM (1993) A time integration algorithm for structural dynamics with improved numerical dissipation: The generalized- α method. *ASME Journal of Applied Mechanics* 60: 371–375.
- Cottone F, Gammaitoni L, Vocca H, et al. (2012) Piezoelectric buckled beams for random vibration energy harvesting. *Smart Materials and Structures* 21(3): 035021.
- Deng Z and Dapino MJ (2014) Characterization and finite element modeling of Galfenol minor flux density loops. *Journal of Intelligent Material Systems and Structures* 1045389X14521703.
- Deng Z and Dapino MJ (2015a) Modeling and design of Galfenol unimorph energy harvesters. *Smart Materials and Structures* 24(12): 125019.
- Deng Z and Dapino MJ (2015b) Multiphysics modeling and design of Galfenol-based unimorph harvesters. Proceedings of SPIE, 9433: 94330B.
- Erturk A, Hoffmann J and Inman DJ (2009) A piezomagnetoelastic structure for broadband vibration energy harvesting. *Applied Physics Letters* 94: 254102.
- Erturk A and Inman DJ (2011) Broadband piezoelectric power generation on high-energy orbits of the bistable duffing oscillator with electromechanical coupling. *Journal of Sound and Vibration* 330(10): 2339–2353.
- Evans PG and Dapino MJ (2010) Efficient magnetic hysteresis model for field and stress application in magnetostrictive Galfenol. *Journal of Applied Physics* 107(6): 063906.
- Ferrari M, Ferrari V, Guizzetti M, et al. (2010) Improved energy harvesting from wideband vibrations by nonlinear piezoelectric converters. *Sensors and Actuators A: Physical* 162(2): 425–431.
- Harne RL and Wang KW (2013) A review of the recent research on vibration energy harvesting via bistable systems. *Smart Materials and Structures* 22(2): 023001.
- Kita S, Ueno T and Yamada S (2015) Improvement of force factor of magnetostrictive vibration power generator for high efficiency. *Journal of Applied Physics* 117: 17B508.
- Moon FC and Holmes PJ (1979) A magnetoelastic strange attractor. *Journal of Sound and Vibration* 65(2): 275–296.
- Rezaealam B, Ueno T and Yamada S (2012) Finite element analysis of Galfenol unimorph vibration energy harvester. *Magnetics, IEEE Transactions on* 48(11): 3977–3980.
- Roundy S, Wright PK and Rabaey J (2003) A study of low level vibrations as a power source for wireless sensor nodes. *Computer Communications* 26(11): 1131–1144.
- Shu L, Dapino MJ, Evans PG, et al. (2011) Optimization and dynamic modeling of Galfenol unimorphs. *Journal of Intelligent Material Systems and Structures* 22(8): 781–793.
- Shu L, Headings LM, Dapino MJ, et al. (2014) Nonlinear model for Galfenol cantilevered unimorphs considering full magnetoelastic coupling. *Journal of Intelligent Material Systems and Structures* 25(2): 187–203.
- Staley ME and Flatau AB (2005) Characterization of energy harvesting potential of Terfenol-D and Galfenol. Proceedings of SPIE 5764: 630–640.
- Ueno T and Yamada S (2011) Performance of energy harvester using iron–gallium alloy in free vibration. *Magnetics, IEEE Transactions on* 47(10): 2407–2409.
- Van Blarigan L, Danzl P and Moehlis J (2012) A broadband vibrational energy harvester. *Applied Physics Letters* 100(25): 253904.
- Yoo J and Flatau AB (2012) A bending-mode Galfenol electric power harvester. *Journal of Intelligent Material Systems and Structures* 23(6): 647–654.
- Zhao X and Lord DG (2006) Application of the Villari effect to electric power harvesting. *Journal of Applied Physics* 99(8): 08M703.